Freeze-thaw decellularization of the trabecular meshwork in an ex vivo eye perfusion model

Yalong Dang [1], **Susannah Waxman** [1], **Chao Wang** [1,2], **Adrianna Jensen** [1], **Ralitsa T Loewen** [1], **Richard A Bilonick** [1], **Nils A Loewen** [Corresp. 1]

[1] Department of Ophthalmology, University of Pittsburgh, Pittsburgh, Pennsylvania, United States

[2] Department of Ophthalmology, Xiangya School of Medicine, Central South University, Changsha, China

Corresponding Author: Nils A Loewen
Email address: loewen.nils@gmail.com

Objective: The trabecular meshwork (TM) is the primary substrate of outflow resistance in glaucomatous eyes. Repopulating diseased TM with fresh, functional TM cells might represent a novel therapeutic breakthrough. Various decellularized TM scaffolds were developed by ablating existing cells with suicide gene therapy or saponin, but always with incomplete cell removal or dissolve the extracellular matrix. We hypothesized that a chemical-free, freeze-thaw method would be able to produce a fully decellularized TM scaffold for cell transplantation.

Materials and Methods: We obtained 24 porcine eyes from a local abattoir, dissected and mounted them in an anterior segment perfusion and pressure transduction system within two hours of sacrifice. After they stabilized for 72 hours, eight eyes each were assigned to freeze-thaw (F) ablation (-80°C×2), to 0.02% saponin (S) treatment, or the control group (C), respectively. The trabecular meshwork was transduced with an eGFP expressing feline immunodeficiency viral (FIV) vector and tracked via fluorescent microscopy to confirm ablation. Following treatment, the eyes were perfused with standard tissue culture medium for 180 hours. We assessed histological changes by hematoxylin and eosin staining. TM cell viability was evaluated with a calcein AM/propidium iodide (PI) assay. We measured IOP and modeled it with a linear mixed effects model using a B-spline function of time with 5 degrees of freedom.

Results: F and S experienced a similar IOP reduction by 30% from baseline (P=0.64). IOP reduction of about 30% occurred in F within 24 hours and in S within 48 hours. Live visualization of eGFP demonstrated that F conferred a complete ablation of all TM cells and only a partial ablation in S. Histological analysis confirmed that no TM cells survived in F while the extracellular matrix remained. The viability assay showed very low PI and no calcein staining in F in contrast to numerous PI-labeled dead TM cells and calcein-labeled viable TM cells in S.

Conclusion: We developed a rapid TM ablation method that uses cyclic freezing that is free of biological or chemical agents and able to produce a decellularized TM scaffold with preserved TM extracellular matrix in an organotypic perfusion culture.

Freeze-thaw decellularization of the trabecular meshwork in an ex vivo eye perfusion model

Alternatives: Trabecular meshwork freeze-thaw decellularization and B-spline effect modeling in perfused pig eyes

B-spline effect modeling of trabecular meshwork freeze-thaw decellularization in perfused pig eyes

Yalong Dang[1], Susannah Waxman[1], Chao Wang[1, 2], Adrianna D. Jensen[1], Ralitsa T. Loewen[1], Richard A. Bilonick[1], Nils A. Loewen[1]

Affiliations:

1: Department of Ophthalmology, School of Medicine, University of Pittsburgh, Pittsburgh, United States of America

2: Department of Ophthalmology, Xiangya School of Medicine, Central South University, Changsha, China

* Corresponding author:
Nils A. Loewen, MD, PhD
203 Lothrop St
Suite 819
Pittsburgh, PA 15213
Email: Loewen.nils@gmail.com
Phone: 412-944-2554

Abstract

Objective: The trabecular meshwork (TM) is the primary substrate of outflow resistance in glaucomatous eyes. Repopulating diseased TM with fresh, functional TM cells might represent a novel therapeutic breakthrough. Various decellularized TM scaffolds were developed by ablating existing cells with suicide gene therapy or saponin, but always with incomplete cell removal or dissolve the extracellular matrix. We hypothesized that a chemical-free, freeze-thaw method would be able to produce a fully decellularized TM scaffold for cell transplantation.

Materials and Methods: We obtained 24 porcine eyes from a local abattoir, dissected and mounted them in an anterior segment perfusion and pressure transduction system within two hours of sacrifice. After they stabilized for 72 hours, eight eyes each were assigned to freeze-thaw (F) ablation (-80°C×2), to 0.02% saponin (S) treatment, or the control group (C), respectively. The trabecular meshwork was transduced with an eGFP expressing feline immunodeficiency viral (FIV) vector and tracked via fluorescent microscopy to confirm ablation. Following treatment, the eyes were perfused with standard tissue culture medium for 180 hours. We assessed histological changes by hematoxylin and eosin staining. TM cell viability was evaluated with a calcein AM/propidium iodide (PI) assay. We measured IOP and modeled it with a linear mixed effects model using a B-spline function of time with 5 degrees of freedom.

Results: F and S experienced a similar IOP reduction by 30% from baseline (P=0.64). IOP reduction of about 30% occurred in F within 24 hours and in S within 48 hours. Live visualization of eGFP demonstrated that F conferred a complete ablation of all TM cells and only a partial ablation in S. Histological analysis confirmed that no TM cells survived in F while the extracellular matrix remained. The viability assay showed very low PI and no calcein staining in F in contrast to numerous PI-labeled dead TM cells and calcein-labeled viable TM cells in S.

Conclusion: We developed a rapid TM ablation method that uses cyclic freezing that is free of biological or chemical agents and able to produce a decellularized TM scaffold with preserved TM extracellular matrix in an organotypic perfusion culture.

Keywords: Trabecular meshwork, decellularization, ablation, intraocular pressure, pig eyes, freeze-thaw, glaucoma

Introduction

The trabecular meshwork (TM) is the primary substrate of outflow resistance in normal and glaucomatous eyes. Recent studies suggested not only low TM cellularity (Alvarado, Murphy & Juster, 1984; Baleriola et al., 2008), but also TM cytoskeleton and phagocytosis changes in primary open angle glaucoma (Clark et al., 1995; Fatma et al., 2009; Izzotti et al., 2010; Saccà, Pulliero & Izzotti, 2015; Peters et al., 2015; Micera et al., 2016). Repopulating diseased TM with fresh, functional TM cells has been shown to restore homeostasis of normal outflow and thus might represent a novel therapeutic breakthrough (Du et al., 2013; Abu-Hassan et al., 2015; Yun et al., 2016; Zhu et al., 2016).

For TM cell transplantation studies, preserving the structure and the extracellular matrix are desirable to provide a natural transplantation environment. Eliminating or reducing the number of host TM cells are also useful. In a recent study, an ex vivo 3D bioengineered TM scaffold repopulated by human primary TM cells was developed, but without the distinct layers of juxtacanalicular, corneoscleral and uveal TM (Torrejon et al., 2016). Transgenic (Tg-MYOC Y437H (Zhu et al., 2016)) and laser photocoagulation mouse models (Yun et al., 2014) have also been used or proposed for TM transplantation, respectively. However, the anatomy of the rodent outflow tract has only a limited number of TM cell layers (three to four) compared to that of humans (Ko & Tan, 2013). Porcine eyes share many features that are similar to human eyes, including size, structure, intraocular pressure (IOP), the outflow pattern (Sanchez et al., 2011; Loewen et al., 2016b,a) and a large trabecular meshwork that guards the angular aqueous plexus (Tripathi, 1971) with Schlemm's canal-like segments (Suárez & Vecino, 2006). The presence of biochemical glaucoma markers in the pig (Suárez & Vecino, 2006), genomic similarities to humans that rival that of mice ("Pairwise Alignment Human vs Pig Blast Results"; Groenen et al., 2012; Flicek et al., 2014) and microphysiological properties such as giant vacuole formation Schlemm's canal endothelium (McMenamin & Steptoe, 1991) suggests pig eyes as glaucoma research models (Ruiz-Ederra et al., 2005).

Abu-Hassan et al. used saponin as an elegant way to induce a glaucoma-like dysfunction and cell loss in the TM of pig eyes (Abu-Hassan et al., 2015) with a 36% ± 9% cell count reduction at 10 minutes. Saponins are a mixed group of plant derived, steroid and terpenoid glycosides that are used as detergents. The impact on remaining host and transplanted donor TM cells as well as on the ECM is not known. To address these concerns, we developed a chemical-free, freeze-thaw method to produce a decellularized TM scaffold. Together with our anterior segment perfusion system (Loewen et al., 2016b), this scaffold model can be used for cell transplantation, allowing real-time TM visualization and IOP measurement.

Materials and Methods

Study Design

Pig eyes were obtained from a local abattoir and prepared for culture within 2 hours of death. Twenty-four eyes were assigned to three groups with eight eyes in each to serve as controls, undergo free-thaw cycles or be infused with saponin. This number was chosen based on past power calculations and the maximum number that could be perfused simultaneously thereby minimizing the variability with same group experiments with our setup (Loewen et al., 2016b,a). Anterior segment perfusion cultures were allowed to stabilize for 72 hours before subject to freeze-thaw cycles or saponin supplemented media, respectively. The intraocular pressure (IOP) was recorded continuously by a pressure transducer system (Physiological Pressure Transducer, SP844; MEMSCAP, Skoppum, Norway) (Loewen et al., 2016b,a). Eyes cultures were continued for another 180 hours. Two additional eyes per ablation method group were transduced with eGFP expressing feline immunodeficiency viral vectors and subjected to the same ablation methods as used in the experimental groups. Expression of eGFP was monitored and compared. Two eyes per group were randomly selected for viability assays and histological analysis.

Preparation of Porcine Anterior Segments and Perfusion System

After removing extraocular tissues, freshly enucleated porcine eyes from a local abattoir (Thoma Meat Market, Saxonburg, PA) were placed into a 5% povidone-iodine solution (NC9771653, Fisher Scientific, Waltham, MA) for 3 minutes and rinsed three times with phosphate-buffered saline (PBS). Eyes were hemisected 7 mm posterior and parallel to the limbus and the lens, ciliary body, and iris were carefully removed. Anterior segments were again washed with PBS three times and mounted in anterior segment perfusion dishes. Media (phenol-free DMEM (SH30284, HyClone, GE Healthcare, UK)) supplemented with 1% fetal bovine serum, and 1% antibiotic-antimycotic (15240062, Thermo Fisher Scientific, Waltham, MA) was continuously pumped into the anterior chambers at a constant infusion rate of 3 microliters per minute. After calibration, the IOP was recorded in 2-minute intervals.

Trabecular Ablation by Freeze-Thaw cycles or 0.02% Saponin

After 72 hours of allowing eyes to stabilize, eyes were subjected to freeze-thaw cycles or 0.02% saponin, respectively. For the freeze-thaw ablation, anterior segments were exposed to -80°C for 2 hours, then thawed at room temperature for 1 hour. After two cycles of freeze-thaw, anterior segments were reconnected to the perfusion system. For the saponin ablation, the conventional perfusion media was replaced with 0.02% saponin supplemented media for 15 minutes, then exchanged for the normal perfusion medium in 37 °C incubator as described before (Abu-Hassan et al., 2015).

Anterior Segment Transduction and TM Visualization

Feline immunodeficiency viral vectors expressing eGFP were generated by transient cotransfection of envelope plasmid pMD.G, packaging plasmid pFP93, and gene-transfer plasmid encoding eGFP and neomycin resistance GINSIN (Saenz et al., 2007; Oatts et al., 2013; Zhang et al., 2014) using a polyethylenimine method (Loewen et al., 2016b). The vector-rich supernatant from transfected 293T cells were harvested two, four and six days after transfection and concentrated by ultracentrifugation. 10^7 transducing units (TU) of GINSIN were injected into the anterior chambers. eGFP expression was followed through the bottom of the culture dish using a dissecting microscope equipped for epifluorescence (SZX16, Olympus, Tokyo, Japan).

TM Viability Analysis and Histology

TM cell viability was assessed by calcein acetoxymethyl (calcein-AM) and propidium iodide (PI) co-labelling (Gonzalez, Hamm-Alvarez & Tan, 2013). After 180 hours, the anterior segments were collected and washed with PBS three times. The limbus with the TM was dissected and incubated with calcein-AM (0.3 µM, C1430, Thermo Fisher, Waltham, MA) and PI (1 µg/ml, P1304MP, Thermo Fisher, Waltham, MA) for 30 min at 37°C. After three additional PBS washes, the TM was flat-mounted and imaged under an upright laser scanning confocal microscope at 400-fold magnification (BX61, Olympus, Tokyo, Japan). Images were captured at three distinct TM depths corresponding to the three meshwork layers, the innermost, uveoscleral, corneoscleral and cribriform TM closest to Schlemm's canal. TM samples obtained from at least two separate quadrants per eye were dissected and fixed with 4% paraformaldehyde in PBS for 24 hours. After rinsing them three times in PBS, they were embedded in paraffin, sectioned at 6-micron thickness and stained with hematoxylin and eosin.

Statistics

Data were presented as the mean ± standard error and analyzed by PASW 18.0 (SPSS Inc., Chicago, IL, USA). One-way ANOVA was performed for the comparison of IOP and TM cellularity among the different groups. Statistical difference was considered significant if $p<0.05$. A linear mixed effects model was fitted to the fold change response in R (Core Team, 2016). The response was modeled as a B-spline function of time with 5 degrees of freedom (Berk; Hu et al., 1998).

Results

Gross morphology and histology

Two eyes per group were discarded due to leaks while the baseline was established. In eyes that were successfully cultured, the gross morphology of the anterior chamber remained well preserved after two freeze-thaw cycles, with light opacification of the cornea as the most notable change (**Fig. 1**). Histology from within 24 hours after exposure to freeze-thaw (F) or

saponin (S) indicated that F preserved the microarchitecture better **(Fig. 2 A and B)** than S **(Fig. 2 C)**. Blue stained nucleoli could still be observed, but disappeared later consistent with the viability assay results described below. There was less extracellular matrix material present in S than in C and F.

Monitoring of TM ablation

Ablation control eyes were transduced with 1×10^7 eGFP FIV vectors before F and S. 24 hours after transduction, the TM cells began to express eGFP, reaching a peak intensity at 48 hours, as reported previously (Loewen et al., 2016b; Dang et al., 2016b). There were discontinuous areas of transduced TM (**Fig. 3 top**) and transduction along corneal stretch folds as well as sclera. Two cycles of -80°C completely abolished eGFP expression. Two cycles were necessary because pilot eyes with only one cycle still showed some eGFP positive cells. In contrast, after 0.02% saponin perfusion, eGFP fluorescence appeared quenched, and only a small portion of transduced cells was ablated 24 hours after exposure (**Fig. 3 bottom**).

Trabecular meshwork viability assay

After two weeks of perfusion, most cells in all three TM layers from the negative control group were labeled by Calcein-AM (**Fig. 4a-Fig. 4c**), while only occasional cells were stained with PI (**Fig. 4b and Fig. 4c**). In contrast, no Calcein-AM staining and very few PI-stained cells were found in the freeze-thaw group (**Fig. 4d-Fig. 4f**). Different from the above two groups, most of the TM cells in S were labeled by PI, with few cells in the uveal and corneoscleral TM demonstrating a light calcein-AM staining (**Fig. 4g-Fig. 4h**).

Intraocular pressure

A stable baseline was established for all anterior segments for 72 hours before F, or S. IOP varied insignificantly by 10.3±7.5 % throughout the end of the study (*Ps*>0.05 compared to the baseline) **(Fig. 5**). However, pressure decreased dramatically after either freeze-thaw or saponin (baseline freeze-thaw 14.75±2.24 mmHg, saponin 14.37± 1.14 mmHg, *P*=0.288). At 12 hours, F dropped to 70% ±7.1% and S to 79.2±8.1% of baseline, respectively. F remained significantly lower than C for 96 hours (p= 0.02), but eye experienced a larger IOP variability onward resulting in reduced significance. In contrast, S had a significantly lower IOP throughout the study until the experimental endpoint at 180 hours. We applied a linear mixed effects model that used a B-spline function of time with 5 degrees of freedom (Berk) **(Fig. 6)**. The results reflect the averages shown in Fig. 5 and confirm the three non-linear behaviors with distinctly different patterns. F had an intercept, representative of the initial IOP drop, that was -0.378 fold less ($p<0.001$) than C and a standard error of 0.088 with 15 degrees of freedom and a t-value of -4.3. F was not significantly different from S in the B-spline function model (p=0.142). S had an intercept that was 0.242 fold less than C (p=0.013) with a standard error of 0.086 and 15 degrees of freedom.

Discussion

In this study, we developed a method to decellularize the trabecular meshwork in anterior segment perfusion cultures quickly and reliably. This was achieved with two cycles of freezing at -80°C and thawing at room temperature. Doing so avoids the use of chemical agents that might dissolve the extracellular matrix or have other, not yet discovered effects. We compared this method to saponin-mediated disruption. Each method has distinct properties and advantages:

Freeze-thaw cycles, applied here to group F, have been used extensively before to ablate tissues in human diseases (Erinjeri & Clark, 2010; Baust et al., 2014; Chu & Dupuy, 2014) including cyclocryodestruction in glaucoma (Benson & Nelson, 1990). It has also been used in research (Baust et al., 2014; Chan & Ooi, 2016; Liu et al., 2016) and in food production ("Fish and Fishery Products Hazards and Controls Guidance"; Gill, 2006; Craig, 2012). The mechanisms of cryoablation in medicine include direct cell injury, vascular injury, ischemia, apoptosis, and immunomodulation (Chu & Dupuy, 2014): cell injury during freezing causes dehydration from the so-called solution effect that causes the earlier freezing extracellular compartment to extract solutes, an osmotic gradient and cell shrinkage (Lovelock, 1953) that can be enhanced by ice crystal formation within the cell, damaging organelles and the cell membrane. During thawing, the intracellular compartment shifts to hypertonia, attracting fluid that causes the cell to burst. Mechanisms not at work in our model presented here are direct cold-induced coagulative necrosis that is the result of sublethal temperatures that activate apoptosis (Baust & Gage, 2005) and direct, cold-induced coagulative necrosis from vascular injury as a result of stasis, thrombosis, and ischemia. An interesting clinical effect is an intense immunogenicity after cryoablation that is different from heat coagulation as immunogenic epitopes are preserved (Jansen et al., 2010).

Saponin, used in experimental group S, can be used to destroy cells through lysis. At lower concentrations, it has been used to reduce the viability of cells (Abu-Hassan et al., 2015). It is an enormously large class of chemical compounds that exists in a range of plant species (Saponaria) which can produce soap-like foam when shaken in aqueous solution and has been used in as detergents (Coombes, 2012). These substances are amphiphilic (both hydro- and lipophilic) glycosides in which sugar is bound to a functional three-terpene group via a glycosidic bond. Saraponins are a significant subset of saponins that are steroidal while aglycone derivatives have pharmacologic characteristics of alkaloids. Historically, saponins have also been used in fishing as a fish poison (Campbell, 1999). In research and treatment, their ability to form complexes with cholesterol to create pores in cell membrane bilayers to induce lysis or enhance penetration of macromolecules has been used (Holmes et al., 2015). These properties may have wide-ranging and difficult to identify effects in cell transplantation models. Each purchased batch may have a different composition of compounds which may make it necessary to

characterize features and concentrations for various lots and could reduce the reproducibility of experiments.

The macroscopic appearance had only relatively minor changes in F and S and included a mild opacification of the cornea. The microscopic architecture was best preserved in F, but less so in S, which can be expected based on the properties of these two different methods described above. Especially the change of permeability of cell membranes by saponin can cause worsened edema by allowing fluids to enter the extracellular space more quickly compared to freeze-thaw that is more likely to results in dehydration. Compared to the cells themselves, many blue nuclei persisted in early histology because they are less permeable and contain less fluid compared to the cytoplasm. These observations were reflected in the ablation of transduced, eGFP expressing cells. Freeze-thaw caused nearly complete loss of fluorescence after the first cycle and disappeared entirely when cells were disrupted after the second cycle. Saponin appears to have caused leakage of eGFP proteins where diminished fluorescence was observed, but only a few cells were fully lysed.

The viability cell confirms our findings from the histological analysis and eGFP ablation. Freeze-thaw caused the disappearance of almost all cells secondary to the above mechanism of cell dehydration and subsequent burst. In our experiments, saponin appears to have caused a sublethal injury to many cells, especially in the uveal and corneoscleral TM. Abu-Hassan et al. have optimized a protocol to induce such sublethal damage from saponin to mimic and treat glaucoma in an ex vivo model (Abu-Hassan et al., 2015). This also matches the slower decline seen in a model of inducible cytoablation mediated by an HSVtk suicide vector (Zhang et al., 2014).

This pattern of cell death matches the IOP reduction of groups F and S. F experienced a more immediate drop compared to S as could be expected by a complete breakdown of the outflow regulation by the TM. In comparison, the slower downslope seen after saponin exposure likely reflects the more gradual cell function decline with eventual cell death. The eventual IOP was lower in S which may represent the loss not only of cells but also of extracellular matrix which could persist in eyes in F to a variable extent and time. Our use of a B-spline function of time provides for the first time function modeling for a biological system of effects in an eye culture model that play out over a period of time rather than the common comparison of single time points which assumes that observations from one time point to the other are largely unrelated (Hu et al., 1998). Handling longitudinal data this way allows for an extension of the standard linear mixed-effects models that can around for a broad range of non-linear behaviors. They are robust to small sample sizes, as well as too noisy observations and missing data.

Consistent with our clinical (Dang et al., 2016c,a) and laboratory findings (Zhang et al., 2014), TM ablation resulted in the reduction of IOP. A (20.80 ± 8.05)% IOP reduction was achieved at 12 hours after saponin treatment, while a greater (30.00 ± 7.13)% IOP reduction was

achieved in the freeze-thaw group. The freeze-thaw cycle removed all the meshwork cells, including corneoscleral and cribriform meshwork cells which account for at least 50% of trabecular outflow resistance, whereas most of these cells were preserved after saponin ablation. It is possible that the IOP reduction seen after cyclocryodestruction is partially due to an improvement of conventional outflow, not just of reduced aqueous humor production or uveoscleral outflow enhancement from inflammation.

Limitations of this study are that cytoablation via freeze-thaw may liberate other, undesirable factors from non-trabecular cells that also die. The argument against a profound impact of those is that the macroscopic and microscopic structures were surprisingly stable for the entire time of 10 days. We only describe an ablation method here but not a repopulation of the trabecular meshwork by cell transplantation.

In conclusion, we developed a fast, inexpensive and reliable method that results in complete ablation of TM cells while the architecture including trabecular beams was well-preserved.

Funding

NEI K08-EY022737

The Initiative to Cure Glaucoma of the Eye and Ear Foundation of Pittsburgh

Reference

Abu-Hassan DW., Li X., Ryan EI., Acott TS., Kelley MJ. 2015. Induced Pluripotent Stem Cells Restore Function in a Human Cell Loss Model of Open-Angle Glaucoma. *Stem cells* 33:751–761.

Alvarado J., Murphy C., Juster R. 1984. Trabecular meshwork cellularity in primary open-angle glaucoma and nonglaucomatous normals. *Ophthalmology* 91:564–579.

Baleriola J., García-Feijoo J., Martínez-de-la-Casa JM., Fernández-Cruz A., de la Rosa EJ., Fernández-Durango R. 2008. Apoptosis in the trabecular meshwork of glaucomatous patients. *Molecular vision* 14:1513–1516.

Baust JG., Gage AA. 2005. The molecular basis of cryosurgery. *BJU international* 95:1187–1191.

Baust JG., Gage AA., Bjerklund Johansen TE., Baust JM. 2014. Mechanisms of cryoablation: clinical consequences on malignant tumors. *Cryobiology* 68:1–11.

Benson MT., Nelson ME. 1990. Cyclocryotherapy: review of cases over 10-year. *The British journal of ophthalmology* 74:103–105.

Berk M. Smoothing-splines Mixed-effects Models in R using the sme Package: a Tutorial.

Campbell PD. 1999. *Survival Skills of Native California*. Gibbs Smith.

Chan JY., Ooi EH. 2016. Sensitivity of thermophysiological models of cryoablation to the thermal and biophysical properties of tissues. *Cryobiology* 73:304–315.

Chu KF., Dupuy DE. 2014. Thermal ablation of tumours: biological mechanisms and advances in therapy. *Nature reviews. Cancer* 14:199–208.

Clark AF., Miggans ST., Wilson K., Browder S., McCartney MD. 1995. Cytoskeletal changes in cultured human glaucoma trabecular meshwork cells. *Journal of glaucoma* 4:183–188.

Coombes AJ. 2012. *The A to Z of Plant Names: A Quick Reference Guide to 4000 Garden Plants*. Timber Press.

Core Team R. 2016. *R: A Language and Environment for Statistical Computing*. Vienna, Austria: R Foundation for Statistical Computing.

Craig N. 2012. Fish tapeworm and sushi. *Canadian family physician Medecin de famille canadien* 58:654–658.

Dang Y., Kaplowitz K., Parikh HA., Roy P., Loewen RT., Francis BA., Loewen NA. 2016a. Steroid-induced glaucoma treated with trabecular ablation in a matched comparison to primary open angle glaucoma. *Clinical & experimental ophthalmology*. DOI: 10.1111/ceo.12796.

Dang Y., Loewen R., Parikh HA., Roy P., Loewen NA. 2016b. Gene transfer to the outflow tract. *Experimental eye research*:044396.

312 Dang Y., Roy P., Bussel II., Loewen RT., Parikh H., Loewen NA. 2016c. Combined analysis of
313 trabectome and phaco-trabectome outcomes by glaucoma severity. *F1000Research* 5:762.

314 Du Y., Yun H., Yang E., Schuman JS. 2013. Stem cells from trabecular meshwork home to TM
315 tissue in vivo. *Investigative ophthalmology & visual science* 54:1450–1459.

316 Erinjeri JP., Clark TWI. 2010. Cryoablation: mechanism of action and devices. *Journal of vascular
317 and interventional radiology: JVIR* 21:S187–91.

318 Fatma N., Kubo E., Toris CB., Stamer WD., Camras CB., Singh DP. 2009. PRDX6 attenuates
319 oxidative stress- and TGFβ-induced abnormalities of human trabecular meshwork cells.
320 *Free radical research* 43:783–795.

321 Fish and Fishery Products Hazards and Controls Guidance

322 Flicek P., Amode MR., Barrell D., Beal K., Billis K., Brent S., Carvalho-Silva D., Clapham P., Coates
323 G., Fitzgerald S., Gil L., Girón CG., Gordon L., Hourlier T., Hunt S., Johnson N., Juettemann T.,
324 Kähäri AK., Keenan S., Kulesha E., Martin FJ., Maurel T., McLaren WM., Murphy DN., Nag R.,
325 Overduin B., Pignatelli M., Pritchard B., Pritchard E., Riat HS., Ruffier M., Sheppard D., Taylor
326 K., Thormann A., Trevanion SJ., Vullo A., Wilder SP., Wilson M., Zadissa A., Aken BL., Birney
327 E., Cunningham F., Harrow J., Herrero J., Hubbard TJP., Kinsella R., Muffato M., Parker A.,
328 Spudich G., Yates A., Zerbino DR., Searle SMJ. 2014. Ensembl 2014. *Nucleic acids research*
329 42:D749–55.

330 Gill CO. 2006. Microbiology of Frozen Foods. In: *Handbook of Frozen Food Processing and
331 Packaging*. crcnetbase.com, 85–100.

332 Gonzalez JM Jr., Hamm-Alvarez S., Tan JCH. 2013. Analyzing live cellularity in the human
333 trabecular meshwork. *Investigative ophthalmology & visual science* 54:1039–1047.

334 Groenen MAM., Archibald AL., Uenishi H., Tuggle CK., Takeuchi Y., Rothschild MF., Rogel-Gaillard
335 C., Park C., Milan D., Megens H-J., Li S., Larkin DM., Kim H., Frantz LAF., Caccamo M., Ahn H.,
336 Aken BL., Anselmo A., Anthon C., Auvil L., Badaoui B., Beattie CW., Bendixen C., Berman D.,
337 Blecha F., Blomberg J., Bolund L., Bosse M., Botti S., Bujie Z., Bystrom M., Capitanu B.,
338 Carvalho-Silva D., Chardon P., Chen C., Cheng R., Choi S-H., Chow W., Clark RC., Clee C.,
339 Crooijmans RPMA., Dawson HD., Dehais P., De Sapio F., Dibbits B., Drou N., Du Z-Q.,
340 Eversole K., Fadista J., Fairley S., Faraut T., Faulkner GJ., Fowler KE., Fredholm M., Fritz E.,
341 Gilbert JGR., Giuffra E., Gorodkin J., Griffin DK., Harrow JL., Hayward A., Howe K., Hu Z-L.,
342 Humphray SJ., Hunt T., Hornshøj H., Jeon J-T., Jern P., Jones M., Jurka J., Kanamori H.,
343 Kapetanovic R., Kim J., Kim J-H., Kim K-W., Kim T-H., Larson G., Lee K., Lee K-T., Leggett R.,
344 Lewin HA., Li Y., Liu W., Loveland JE., Lu Y., Lunney JK., Ma J., Madsen O., Mann K.,
345 Matthews L., McLaren S., Morozumi T., Murtaugh MP., Narayan J., Nguyen DT., Ni P., Oh S-J.,
346 Onteru S., Panitz F., Park E-W., Park H-S., Pascal G., Paudel Y., Perez-Enciso M., Ramirez-
347 Gonzalez R., Reecy JM., Rodriguez-Zas S., Rohrer GA., Rund L., Sang Y., Schachtschneider K.,
348 Schraiber JG., Schwartz J., Scobie L., Scott C., Searle S., Servin B., Southey BR., Sperber G.,
349 Stadler P., Sweedler JV., Tafer H., Thomsen B., Wali R., Wang J., Wang J., White S., Xu X.,
350 Yerle M., Zhang G., Zhang J., Zhang J., Zhao S., Rogers J., Churcher C., Schook LB. 2012.
351 Analyses of pig genomes provide insight into porcine demography and evolution. *Nature*

491:393–398.

Holmes SE., Bachran C., Fuchs H., Weng A., Melzig MF., Flavell SU., Flavell DJ. 2015. Triterpenoid saponin augmention of saporin-based immunotoxin cytotoxicity for human leukaemia and lymphoma cells is partially immunospecific and target molecule dependent. *Immunopharmacology and immunotoxicology* 37:42–55.

Hu FB., Goldberg J., Hedeker D., Flay BR., Pentz MA. 1998. Comparison of Population-Averaged and Subject-Specific Approaches for Analyzing Repeated Binary Outcomes. *American journal of epidemiology* 147:694–703.

Izzotti A., Saccà SC., Longobardi M., Cartiglia C. 2010. Mitochondrial damage in the trabecular meshwork of patients with glaucoma. *Archives of ophthalmology* 128:724–730.

Jansen MC., van Hillegersberg R., Schoots IG., Levi M., Beek JF., Crezee H., van Gulik TM. 2010. Cryoablation induces greater inflammatory and coagulative responses than radiofrequency ablation or laser induced thermotherapy in a rat liver model. *Surgery* 147:686–695.

Ko MK., Tan JCH. 2013. Contractile markers distinguish structures of the mouse aqueous drainage tract. *Molecular vision* 19:2561–2570.

Liu X., Zhao G., Shu Z., Niu D., Zhang Z., Zhou P., Cao Y., Gao D. 2016. Quantification of Intracellular Ice Formation and Recrystallization During Freeze-Thaw Cycles and Their Relationship with the Viability of Pig Iliac Endothelium Cells. *Biopreservation and biobanking* 14:511–519.

Loewen RT., Brown EN., Roy P., Schuman JS., Sigal IA., Loewen NA. 2016a. Regionally Discrete Aqueous Humor Outflow Quantification Using Fluorescein Canalograms. *PloS one* 11:e0151754.

Loewen RT., Roy P., Park DB., Jensen A., Scott G., Cohen-Karni D., Fautsch MP., Schuman JS., Loewen NA. 2016b. A Porcine Anterior Segment Perfusion and Transduction Model With Direct Visualization of the Trabecular Meshwork. *Investigative ophthalmology & visual science* 57:1338–1344.

Lovelock JE. 1953. The haemolysis of human red blood-cells by freezing and thawing. *Biochimica et biophysica acta* 10:414–426.

McMenamin PG., Steptoe RJ. 1991. Normal anatomy of the aqueous humour outflow system in the domestic pig eye. *Journal of anatomy* 178:65–77.

Micera A., Quaranta L., Esposito G., Floriani I., Pocobelli A., Saccà SC., Riva I., Manni G., Oddone F. 2016. Differential Protein Expression Profiles in Glaucomatous Trabecular Meshwork: An Evaluation Study on a Small Primary Open Angle Glaucoma Population. *Advances in therapy* 33:252–267.

Oatts JT., Zhang Z., Tseng H., Shields MB., Sinard JH., Loewen NA. 2013. In vitro and in vivo comparison of two suprachoroidal shunts. *Investigative ophthalmology & visual science* 54:5416–5423.

389 Pairwise Alignment Human vs Pig Blast Results. *Available at*
390 *http://useast.ensembl.org/info/genome/compara/mlss.html?mlss=716* (accessed August
391 17, 2015).

392 Peters JC., Bhattacharya S., Clark AF., Zode GS. 2015. Increased Endoplasmic Reticulum Stress in
393 Human Glaucomatous Trabecular Meshwork Cells and Tissues. *Investigative ophthalmology*
394 *& visual science* 56:3860–3868.

395 Ruiz-Ederra J., García M., Martín F., Urcola H., Hernández M., Araiz J., Durán J., Vecino E. 2005.
396 Comparison of three methods of inducing chronic elevation of intraocular pressure in the
397 pig (experimental glaucoma). *Archivos de la Sociedad Espanola de Oftalmologia* 80:571–
398 579.

399 Saccà SC., Pulliero A., Izzotti A. 2015. The dysfunction of the trabecular meshwork during
400 glaucoma course. *Journal of cellular physiology* 230:510–525.

401 Saenz D., Barraza R., Loewen N., Teo W., Kemler I., Poeschla E. 2007. Production and Use of
402 Feline Immunodeficiency Virus (FIV)-Based Lentiviral Vectors. In: Friedmann T, Rossi JJ eds.
403 *Gene Transfer: Delivery and Expression of DNA and RNA : a Laboratory Manual*. CSHL Press,
404 57–73.

405 Sanchez I., Martin R., Ussa F., Fernandez-Bueno I. 2011. The parameters of the porcine eyeball.
406 *Graefe's archive for clinical and experimental ophthalmology = Albrecht von Graefes Archiv*
407 *fur klinische und experimentelle Ophthalmologie* 249:475–482.

408 Suárez T., Vecino E. 2006. Expression of endothelial leukocyte adhesion molecule 1 in the
409 aqueous outflow pathway of porcine eyes with induced glaucoma. *Molecular vision*
410 12:1467–1472.

411 Torrejon KY., Papke EL., Halman JR., Stolwijk J., Dautriche CN., Bergkvist M., Danias J., Sharfstein
412 ST., Xie Y. 2016. Bioengineered glaucomatous 3D human trabecular meshwork as an in vitro
413 disease model. *Biotechnology and bioengineering* 113:1357–1368.

414 Tripathi RC. 1971. Ultrastructure of the exit pathway of the aqueous in lower mammals:(A
415 preliminary report on the "angular aqueous plexus"). *Experimental eye research* 12:311–
416 314.

417 Yun H., Lathrop KL., Yang E., Sun M., Kagemann L., Fu V., Stolz DB., Schuman JS., Du Y. 2014. A
418 laser-induced mouse model with long-term intraocular pressure elevation. *PloS one*
419 9:e107446.

420 Yun H., Zhou Y., Wills A., Du Y. 2016. Stem Cells in the Trabecular Meshwork for Regulating
421 Intraocular Pressure. *Journal of ocular pharmacology and therapeutics: the official journal*
422 *of the Association for Ocular Pharmacology and Therapeutics* 32:253–260.

423 Zhang Z., Dhaliwal AS., Tseng H., Kim JD., Schuman JS., Weinreb RN., Loewen NA. 2014. Outflow
424 tract ablation using a conditionally cytotoxic feline immunodeficiency viral vector.
425 *Investigative ophthalmology & visual science* 55:935–940.

426 Zhu W., Gramlich OW., Laboissonniere L., Jain A., Sheffield VC., Trimarchi JM., Tucker BA., Kuehn

MH. 2016. Transplantation of iPSC-derived TM cells rescues glaucoma phenotypes in vivo. *Proceedings of the National Academy of Sciences of the United States of America*. DOI: 10.1073/pnas.1604153113.

Figures

Figure 1

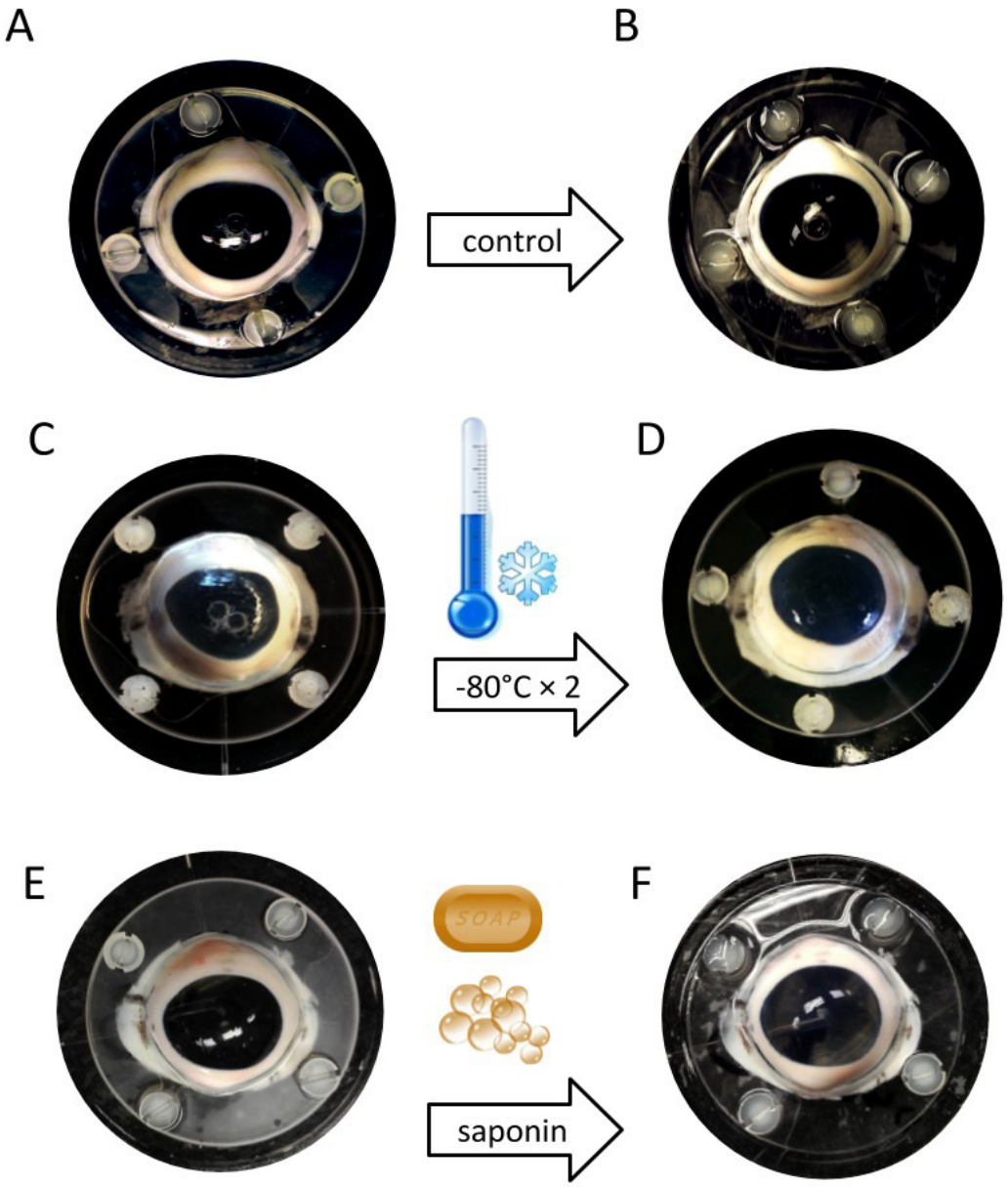

Figure 1: Freeze-thaw treatment of anterior segment cultures. Eyes were exposed to two cycles of freezing at -80°C followed by thawing at room temperature. The macroscopic appearance remained mostly unchanged.

435 **Figure 2**

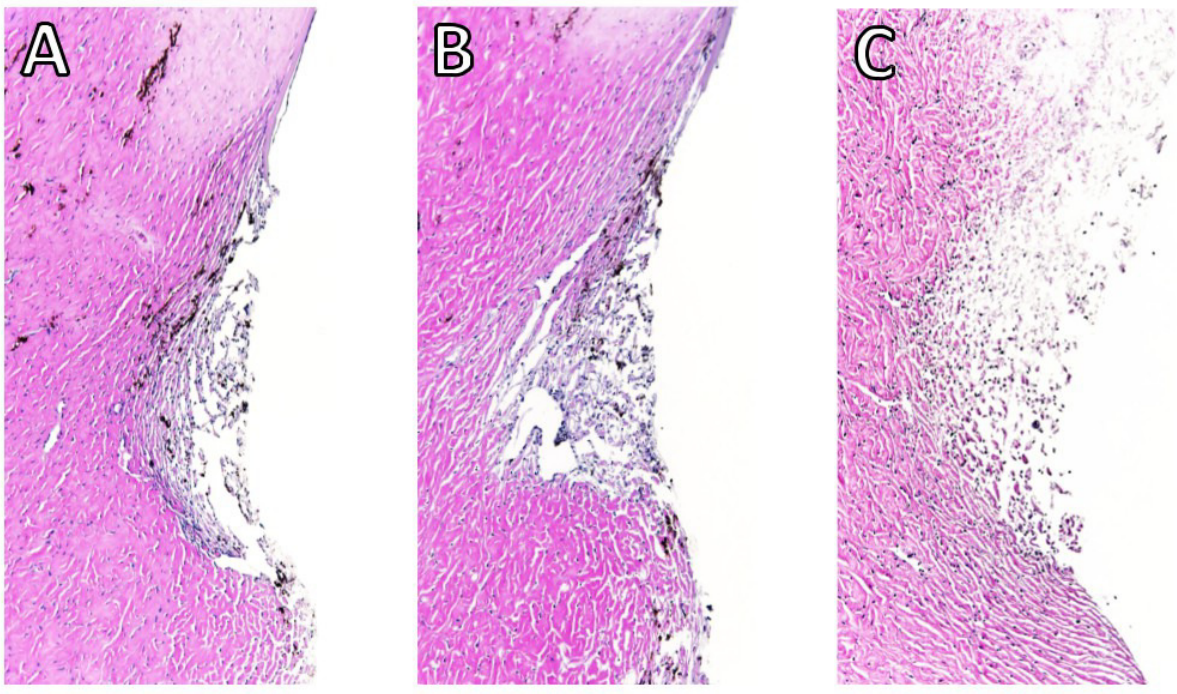

436 **Figure 2. Histology of the angle of perfused anterior chambers.** A) Control eyes had a similar
437 appearance to free-thaw treated eyes (B) in early histology slides. C) Saponin treated eyes. Blue
438 nuclei can be seen in all sections at 24 hours.

439 **Figure 3**

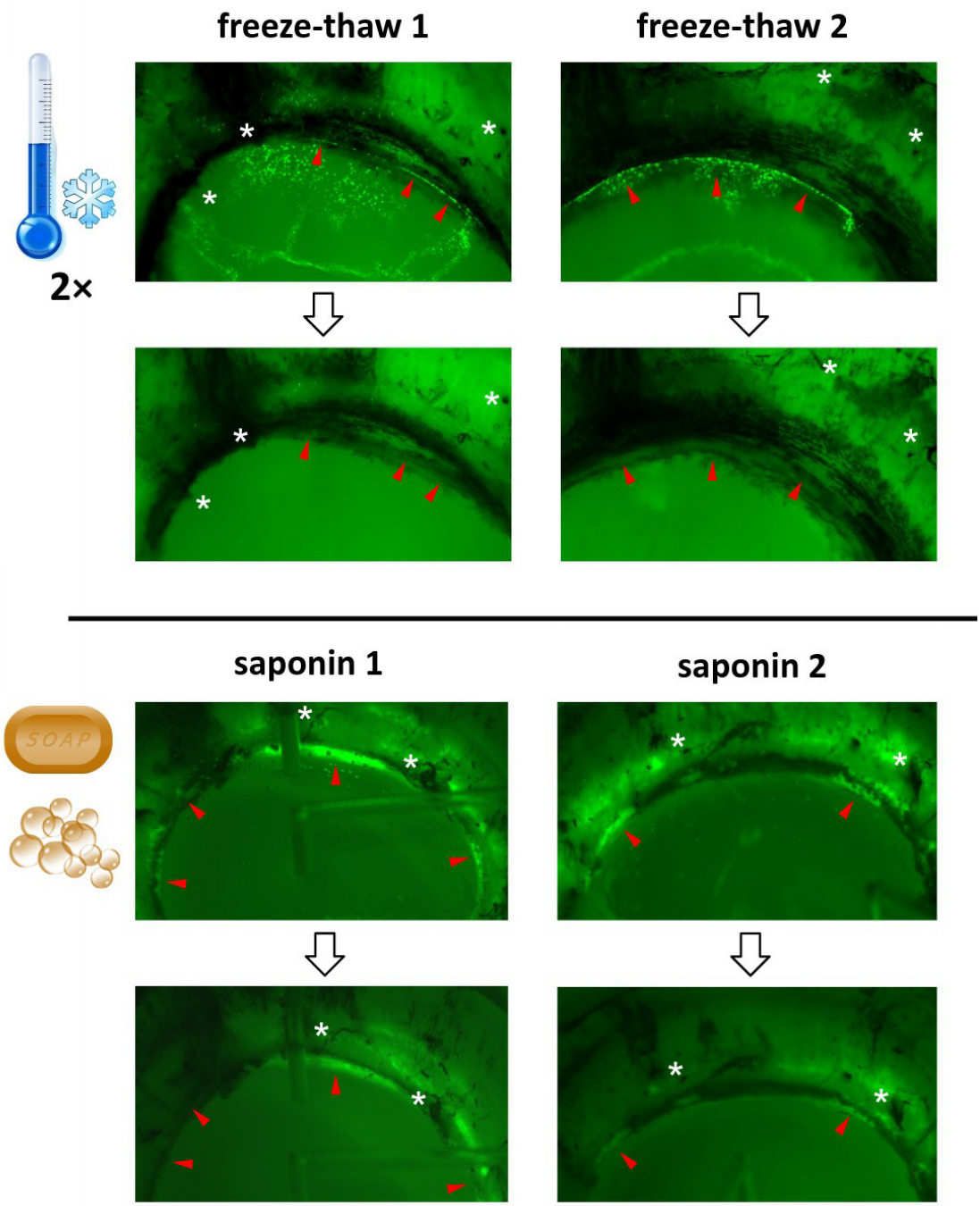

440 **Figure 3: Confirmation of cytoablation.** Fluorescence of eGFP expressing, FIV GINSIN transduced
441 cells vanished completely after two freeze-thaw cycles (top). In contrast, eGFP can still be seen
442 in many transduced cells but at a reduced intensity in saponin-treated eyes (bottom). Red
443 arrowheads point to transduced trabecular meshwork that is ablated completely after freeze-
444 thaw but only diminished in saponin eyes. White asterisks indicate landmarks that can easily be
445 recognized before and after treatment.

446 **Figure 4**

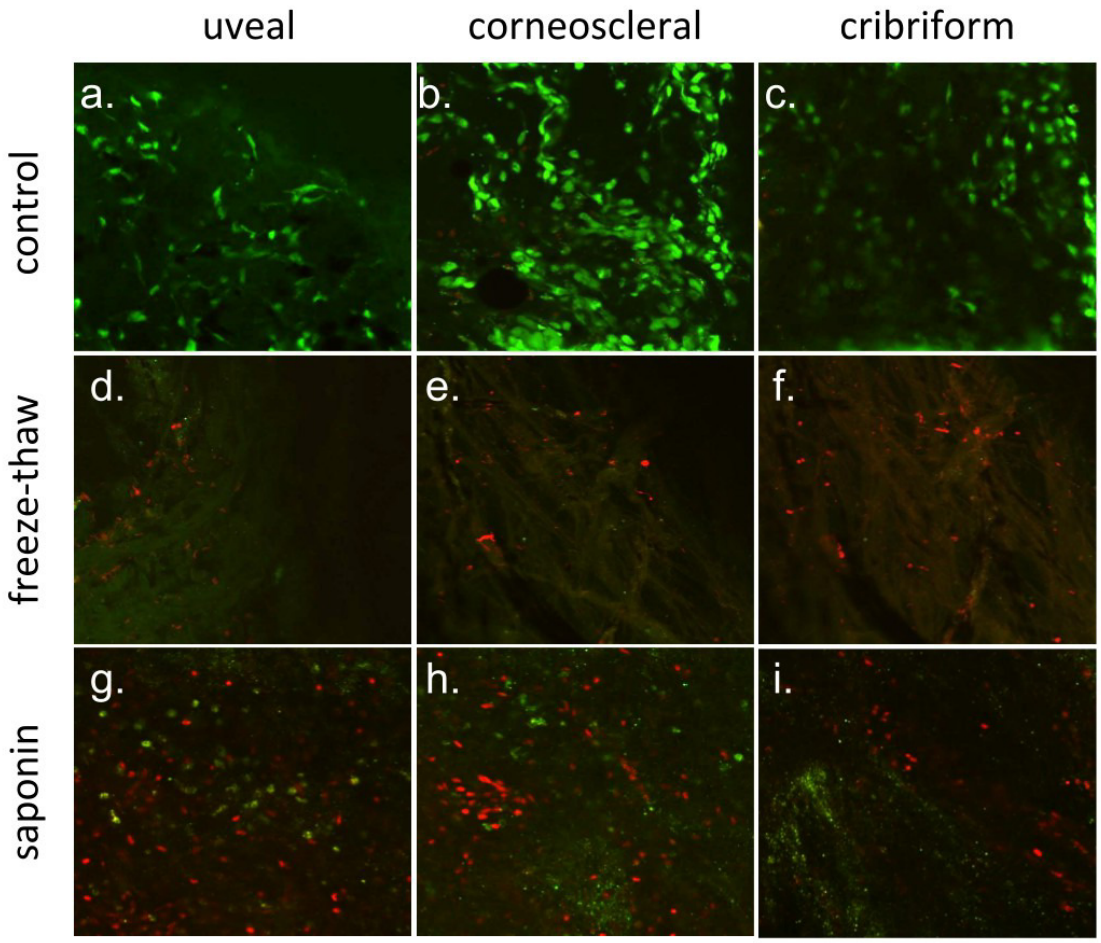

447 **Figure 4. Assessment of TM cell viability by calcein AM/PI co-labelling.** Viable trabecular
448 meshwork (TM) cells exposed to calcein AM showed bright green fluorescence, while dead TM
449 cells allowed PI to enter cell membrane and label the cell nuclear with red fluorescence . In the
450 control group, most TM cells were still viable after perfusion for two weeks (a-c). In contrast,
451 cells, including many nuclei, were destroyed by freeze-thaw. No Calcein AM and only a few PI-
452 labeled TM cells were found (Figure 5d- Figure 5f). Different from the other two groups, a few
453 TM cells were still alive in the uveal TM and corneoscleral TM (g-h), but most of them were
454 labeled as dead cells by PI.

455 **Figure 5**

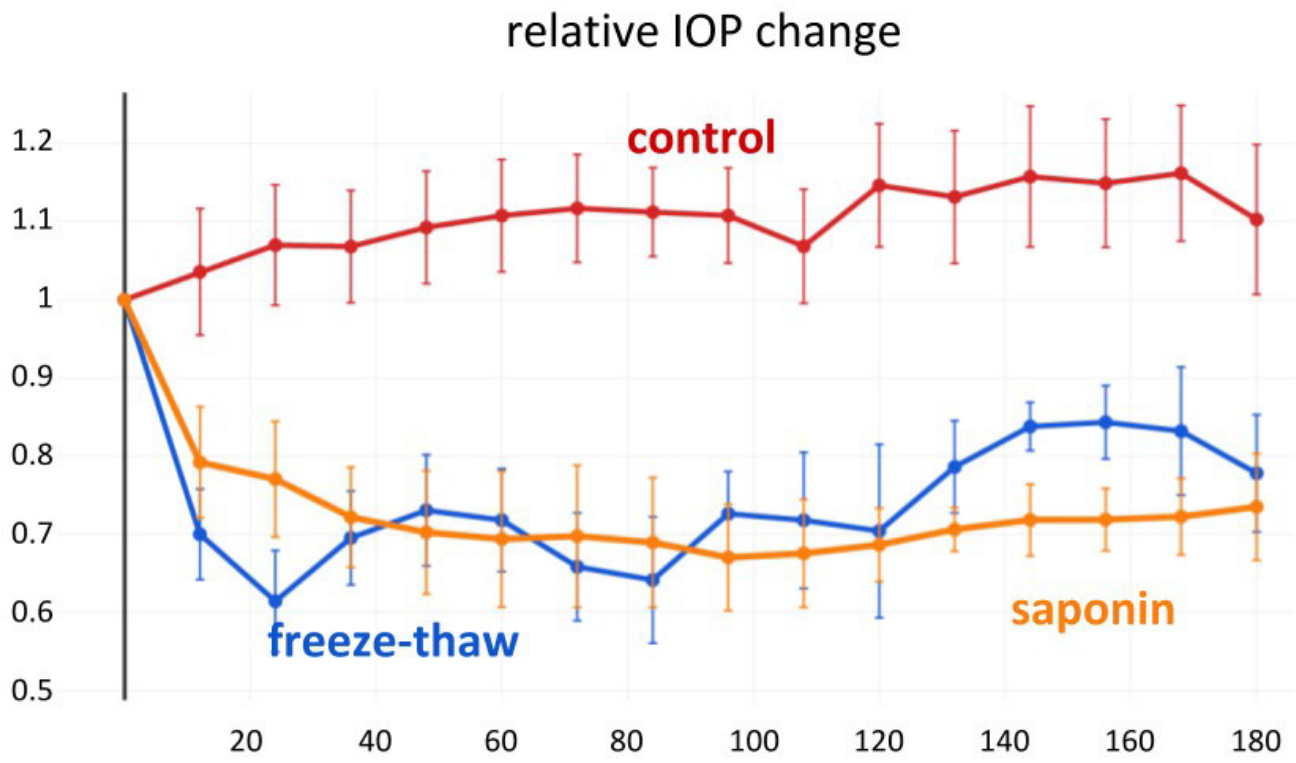

456 **Figure 5. IOP Reduction after TM decellularization.** Freeze-thaw (F) resulted in a more rapid IOP
457 reduction than saponin (S) (averages ± SEM). There were no differences at any single time
458 between F and S. Differences between controls and S were not significant onward from 96
459 hours.

460 **Figure 6**

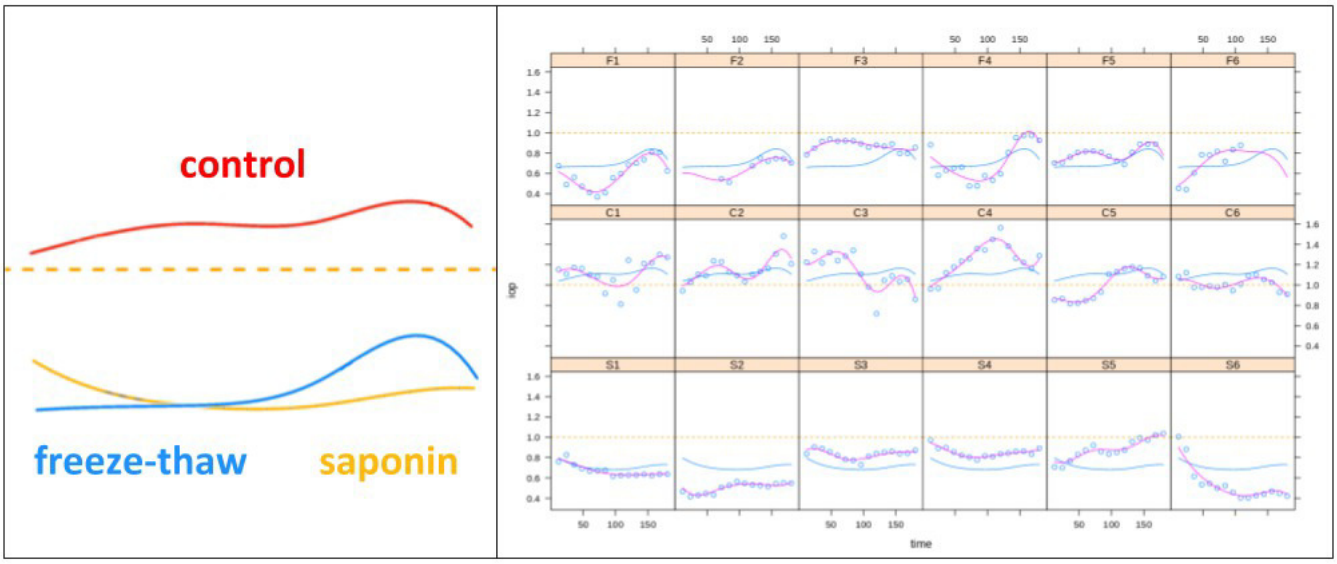

461 **Figure 6: The B-spline function of time with 5 degrees of freedom.** The B-spline consensus
462 function (left) matched the average IOP changes but allowed to better highlight the response
463 patterns despite a considerable data scatter in the individual curves (right; B-splines shown as
464 blue lines).